Mineralogical Magazine, August 2012, Vol. 76(4), pp. 949–962

Phase transitions in hydroxide perovskites: a Raman spectroscopic study of stottite, $FeGe(OH)_6$, to 21 GPa

A. K. Kleppe[1,*], M. D. Welch[2], W. A. Crichton[3] and A. P. Jephcoat[4]

[1] Diamond Light Source, Harwell Science and Innovation Campus, Didcot, Oxfordshire OX11 0DE, UK
[2] Department of Mineralogy, The Natural History Museum, Cromwell Road, London SW7 5BD, UK
[3] European Synchrotron Radiation Facility, 6 rue Jules Horowitz, BP 220, Grenoble Cedex, F-38043, France
[4] Department of Earth Sciences University of Oxford, South Parks Road, Oxford OX1 3AN, UK

[*Received 19 January 2012; Accepted 8 March 2012; Associate Editor: G. Diego Gatta*]

ABSTRACT

The effect of pressure on the naturally occurring hydroxide-perovskite stottite, $FeGe(OH)_6$, has been studied *in situ* by micro-Raman spectroscopy to 21 GPa at 300 K. The ambient spectrum contains six OH-stretching bands in the range 3064−3352 cm^{-1}. The presence of six non-equivalent OH groups is inconsistent with space group $P4_2/n$. In view of this inconsistency a new ambient structure determination of stottite from Tsumeb was carried out, but this did not allow the clear rejection of $P4_2/n$ symmetry. However, a successful refinement was also carried out in space group $P2/n$, a subgroup of $P4_2/n$, which allows for six non-equivalent O atoms. The two refinements are of comparable quality and do not allow a choice to be made based purely on the X-ray data. However, taken with the ambient and 150 K Raman spectra, a good case can be made for stottite having $P2/n$ symmetry at ambient conditions. On this basis, the pressure induced spectroscopic changes are interpreted in terms of a reversible phase transition $P2/n \leftrightarrow P4_2/n$.

Keywords: stottite, hydroxide perovskites, high-pressure, diamond-anvil cell, Raman spectroscopy, X-ray diffraction.

Introduction

Hydroxide-perovskites are A-site empty, perovskite-structured, charge-neutral frameworks of corner-linked $B(OH)_6$ and $B'(OH)_6$ cation octahedra in which all of the oxygen atoms form OH groups, giving a general stoichiometry $BB'(OH)_6$. The H atoms form hydrogen bonds across the faces of the dodecahedral A-site cavity. These structures provide a rare opportunity to study the deformation of a perovskite-type framework in the absence of interactions with an A cation.

The framework can accommodate homovalent and heterovalent cations. All heterovalent hydroxide-perovskites, $BB'(OH)_6$, have ordered frameworks in which different cations alternate on crystallographically non-equivalent sites, examples include schoenfliesite, $MgSn(OH)_6$; burtite, $CaSn(OH)_6$; stottite, $FeGe(OH)_6$; and mopungite, $NaSb(OH)_6$. The ordering of the heterovalent cations is dictated by bond-valence constraints on bridging O atoms, each of which is bonded to an H atom as OH. Disorder in the heterovalent structures is prohibited by under-bonding or over-bonding of these O atoms: e.g. Mg−O−Mg + O−H = 1.67 valence units (vu); Sn−O(H)−Sn + O−H = 2.33 vu; compared with Mg−O−Sn + O−H = 0.33 + 0.67 + 1 = 2 vu. The structures of burtite and stottite are shown in Fig. 1. Burtite and schoenfliesite are the only members of the group for which H atoms have been located (by neutron powder diffraction).

With one exception, mushistonite $CuSn(OH)_6$ (tetragonal, $P4_2/n$), all known stannate hydroxide-perovskites are cubic (space group $Pn\bar{3}$ or $Pn\bar{3}m$) with two non-equivalent H atoms. Stottite,

* E-mail: annette.kleppe@diamond.ac.uk
DOI: 10.1180/minmag.2012.076.4.11

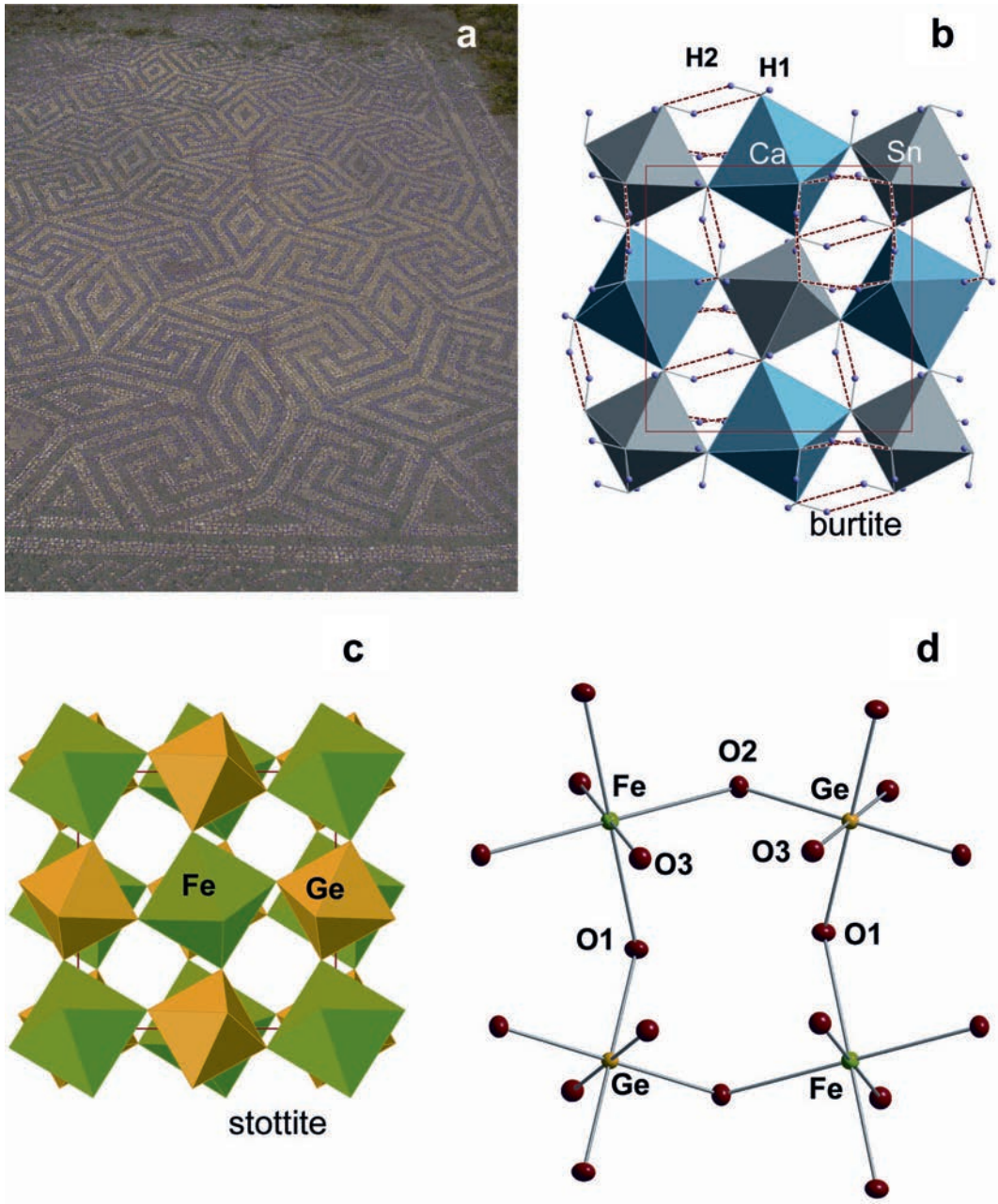

FIG. 1. (*a*) The structural motif of hydroxide-perovskites anticipated in a first century Roman mosaic from Ostia, Italy. (*b*) The structure of burtite, $CaSn(OH)_6$, (Basciano *et al*., 1998), space group $Pn\bar{3}$; O−H···O linkages across the faces of the vacant A site are shown. Burtite has two non-equivalent H atoms. (*c*) The structure of stottite (Ross *et al*., 1988) viewed parallel to the 4_2 axes; H atom positions in stottite are yet to be determined. (*d*) Ball-and-spoke rendition of the structure of stottite indicating the atom sites.

$FeGe(OH)_6$ (Strunz *et al*., 1958; Strunz and Giglio, 1961; Ross *et al*., 1988) and mopungite, $NaSb(OH)_6$ (Williams, 1985) are reported to be tetragonal in space group $P4_2/n$ with three non-equivalent H atoms. Three natural homovalent hydroxide-perovskites have been described: bernalite, $Fe(OH)_3$ (Birch *et al*., 1993; Welch *et al*. 2005); dzahlindite, $In(OH)_3$; and söhngeite, $Ga(OH)_3$. The last two have $Im\bar{3}$ symmetry, whereas bernalite is orthorhombic. The space group of bernalite remains uncertain, although it is primitive (e.g. *Pmmn*; Welch *et al*., 2005) and not *Immm* (Birch *et al*., 1993). Synthetic δ-$Al(OH)_3$ (Matsui *et al*., 2011) is orthorhombic with space group $P2_12_12_1$, and has a single Al site. Wunder *et al*. (2011) reported that the synthetic high-pressure ''3.65 Å-phase'', $MgSi(OH)_6$, is also an hydroxide-perovskite. Originally, the space group was determined as orthorhombic, *Pnam*, but it has been shown subsequently to be monoclinic $P2_1$ by density-functional theory (Wunder *et al*. 2012), or monoclinic $P2_1/n$ by single-crystal XRD (Welch and Wunder, in press).

As expected, hydroxide-perovskites are much more compressible than perovskites, due to the absence of an A cation which is the primary stiffening component of the perovskite structure (Zhao *et al*., 2004). For example, bernalite $Fe(OH)_3$ has K_0 = 75 GPa (Welch *et al*., 2005), compared with $GdFeO_3$ perovskite which has K_0 = 182 GPa (Ross *et al*., 2004). Ross *et al*. (2002) determined the bulk and axial moduli of stottite ($P4_2/n$) to 8 GPa at 300 K by single-crystal XRD as follows: K_0 = 78.4 GPa, (K_0' = 6.2); $K_0(a)$ = 81.3 GPa, (K_0' = 6.4); $K_0(c)$ = 73.3 GPa, (K_0' = 5.7). No evidence for transitional behaviour was observed in this pressure range. The bulk modulus of stottite is very similar to the bulk moduli of $MgSn(OH)_6$ (72 GPa), $ZnSn(OH)_6$ (73 GPa), $Fe(OH)_3$ (78 GPa) and $MgSi(OH)_6$ (76 GPa).

Zhao *et al*. (2004) developed a novel approach to predicting the high-*P* behaviour of perovskites that is based upon bond-valence analysis correlated with the volume behaviour (compressibility) of the dodecahedrally coordinated A site and the octahedrally coordinated B site. Briefly, their analysis of the published structures and bulk moduli of diverse 3:3 perovskites in the literature indicated that those with $\beta_A/\beta_B > 1$ become more distorted with increasing *P*, whereas those with $\beta_A/\beta_B < 1$ become less distorted and can undergo *P*-induced phase transitions. On this basis, as hydroxide-perovskites have vacant and A sites which are very compressible, we would expect them to distort primarily by A-site compression. However, it is conceivable that a limit to compression by rigid rotation of the octahedrally coordinated B site will be reached at some pressure because the non-bonded B−B′ distances shorten considerably in highly rotated structures. If there is such a limit to rigid rotation, we might expect a switch to B−O and B′−O bond shortening as the dominant compression mechanism. According to Zhao *et al*. (2004) such behaviour may lead to phase transitions at high pressure in low-symmetry structures. Hydroxide-perovskites provide a means of testing such ideas, with the additional interest provided by H-mediated interactions.

In this context, our motivation here is to recognize changes in the compression mechanism of hydroxide-perovskites, to understand their compositional dependencies and, ultimately, to identify their structural origins. We have chosen to study stottite, $FeGe(OH)_6$, as it is tetragonal and has the potential to transform on compression and also because high quality natural crystals are available. No synthetic stottite analogues are available and no synthesis recipes have been reported.

The structure of stottite was first determined by Strunz and Giglio (1961) who reported it to be tetragonal in space group $P4_2/n$. This structure has three non-equivalent O atoms, which implies three non-equivalent H atoms, but the H atom positions have yet to be located. Ross *et al*. (1988), also reported $P4_2/n$ symmetry, but expressed significant reservations about assigning tetragonal symmetry to stottite. However, they felt that the single-crystal XRD data did not fully justify assigning lower symmetry. Ross *et al*. (1988) noted that Strunz *et al*. (1958) reported a biaxial optical character for stottite. There is, consequently, some doubt about the true symmetry of stottite that X-ray diffraction may have difficulty in resolving.

Experimental

Raman spectroscopy

The stottite crystal used in this experiment was taken from the same locality as that studied by Ross *et al*. (2002), from the Tsumeb mine in Namibia. This sample was generously donated for study by Mr William Pinch of Rochester, New York, USA. The crystal used in this study is a dark brown single-crystal fragment, 42 × 50 μm in size, which is free from inclusions and wedge-

shaped with a thickness varying from 5–25 μm (Fig. 2). Unpolarized Raman spectra were collected at <300 K at atmospheric pressure, and at increasing and decreasing pressures at 300 K.

For the high-pressure experiment the crystal was mounted in a diamond-anvil cell (DAC) with a ruby sphere for pressure calibration. Synthetic diamonds from Sumitomo Europe with 0.6 mm culets and a stainless steel gasket pre-indented to 50 μm with a 150 μm hole drilled in it were used. The ruby sphere was 8.5 μm in diameter. Fluid helium was used as a pressure-transmitting medium at 0.2 GPa using the gas-loading technique described by Jephcoat *et al*. (1987).

All of the Raman spectra were recorded in 135º scattering geometry using a SPEX Triplemate equipped with a back-illuminated, liquid-N_2-cooled CCD detector in the range of 100 to 4000 cm^{-1}. The intrinsic resolution of the spectrometer is 1.5 cm^{-1} and calibrations are accurate to ±1 cm^{-1}. For some of the bands the fitted peak position varied outside the intrinsic limits of accuracy due to the large full width at half maximum (FWHM) and/or strong band overlap. In particular, the OH-stretching bands at <3200 cm^{-1} at atmospheric pressure overlap and broaden significantly under pressure: their FWHM increases from 80–90 cm^{-1} to 130 cm^{-1} at 5.06 GPa limiting the accuracy in band position to ±15–20 cm^{-1}.

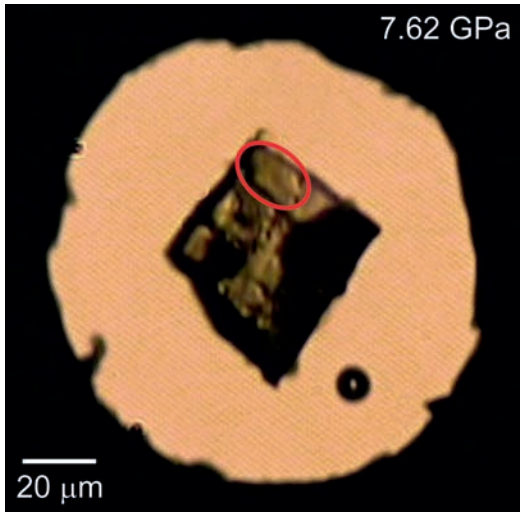

FIG. 2. View into the DAC through the cylinder diamond onto the stottite crystal fragment and ruby sphere in helium at 7.62 GPa. The area of the crystal fragment that was mainly probed in the high-pressure experiment is indicated by a red oval.

The Raman spectra were excited by the 514.5 nm line of an argon ion laser, focussed to a 10 μm diameter spot on the sample. The laser power (<80 mW) was low enough to avoid heating the sample. Ambient Raman spectra were collected in air from different parts of the crystal fragment at varying beam orientations. Raman spectra at pressures of up to 21.1 GPa were obtained from the area marked by a red oval in Fig. 2. This area of the crystal surface appeared optically flat and, for the 135º scattering geometry of the DAC experiment, gave the best intensity and resolution for the OH-stretching modes. The frequency of each Raman band was obtained by fitting Voigtian line profiles.

In the low-temperature Raman experiment a single-crystal fragment of stottite was mounted in a liquid He cooled optical microscope cryostat (Microstat® He, Oxford Instruments) equipped with a Spectrosil water-free window. The crystal was pressed in indium to ensure good thermal contact with the cold finger and the temperature was controlled within ±0.5 K.

Single-crystal X-ray diffraction

A tabular crystal of stottite (0.086 × 0.189 × 0.202 mm) of good optical and diffraction quality from the same locality as that of the crystal studied by Ross *et al*. (2002) was mounted on an XcaliburE kappa-diffractometer operating at 50 kV/45 mA using Mo$K\alpha$ radiation (λ = 0.71073 Å). A CCD-based EOS detector was used for data collection. Unit-cell parameters were refined from 2408 reflections having $I > 7\sigma(I)$. More than a sphere of reflection intensities was collected from 3.8–30.1º θ to a resolution of 0.77 Å. A Lorentz-polarization correction was applied. A Gaussian absorption correction based upon face-indexing was used (μ = 10.39 mm^{-1}) and the reflection intensities converted to structure factors using *CrysalisPro* software (Agilent Technologies). Structure solution and refinement were carried out using the *SHELX* suite of programs (Sheldrick, 2008).

Results

Raman spectroscopy

Ambient Raman spectrum

The ambient Raman spectrum of stottite is shown in Fig. 3. The relative band intensities

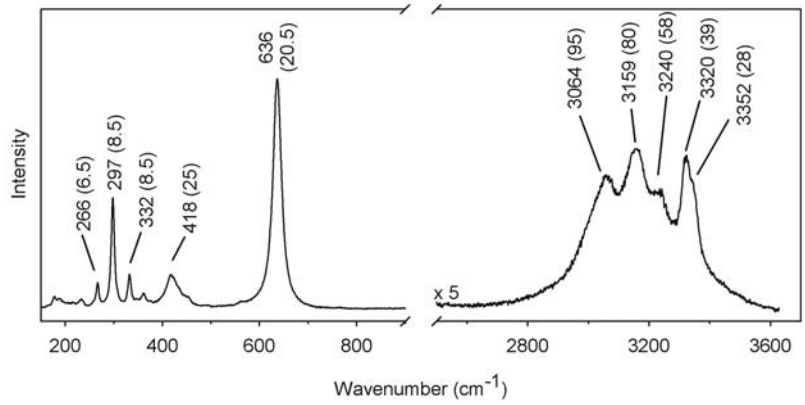

FIG. 3. The ambient Raman spectrum of stottite. The peak positions of the most intense modes are labelled and their full width at half maximum is given in parentheses.

depend upon the orientation of the crystal relative to the incident laser beam. The minimum number of peaks needed to fit the spectra in the OH-stretching region is five: three broad bands centred at 3064, 3159, 3240 cm^{-1}; and two narrow bands centred at 3320 and 3352 cm^{-1}. However, the shape of the 3064 cm^{-1} band suggests two components. To clarify this, spectra were collected at temperatures <300 K. The spectrum at 150 K is shown in Fig. 4. The two-component structure of the 3064 cm^{-1} feature is evident (Fig. 4, bands 5 and 6). The remaining four bands are well resolved in the 150 K spectrum and correlate with their ambient temperature counterparts.

High-pressure Raman spectra

In fitting the high-pressure spectra in the OH-stretching frequency range of stottite we recognize that those spectra that are readily identifiable as related to the ambient spectrum are adequately fitted with five bands, although the broad low-wavenumber band actually consists of two unresolved bands (Fig. 4). Representative Raman spectra of stottite as a function of pressure are shown in Fig. 5. The variation with pressure of OH-stretching bands is shown in Fig. 6 and summarized in Table 1.

The most striking feature on compression is the appearance of three new OH-stretching bands above 9.5 GPa. Furthermore, the 9.5 GPa spectrum appears to contain the three new bands (indicated by blue arrows in Fig. 5*b*) as part of a mixed spectrum that also contains a major contribution from the original five-band spectrum.

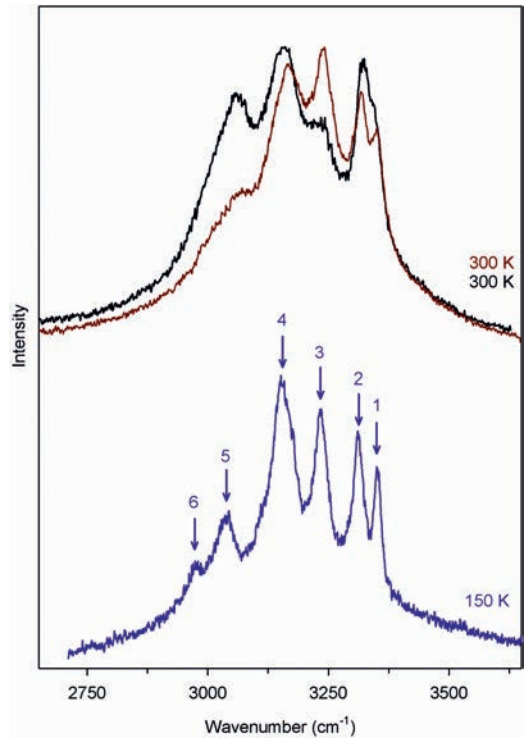

FIG. 4. Raman spectra of the OH-stretching modes of stottite at 150 K and 300 K. Six OH-stretching modes are resolved at 150 K; five of these can be resolved at room temperature. The 300 K spectra were collected outside the diamond-anvil cell and with a 90º difference in crystal-to-laser beam orientation. The low temperature spectrum was measured in a microscope cryostat. The black spectrum was measured using an 1800 g grating and the red and blue spectrum using a 1200 g grating in the spectrometer.

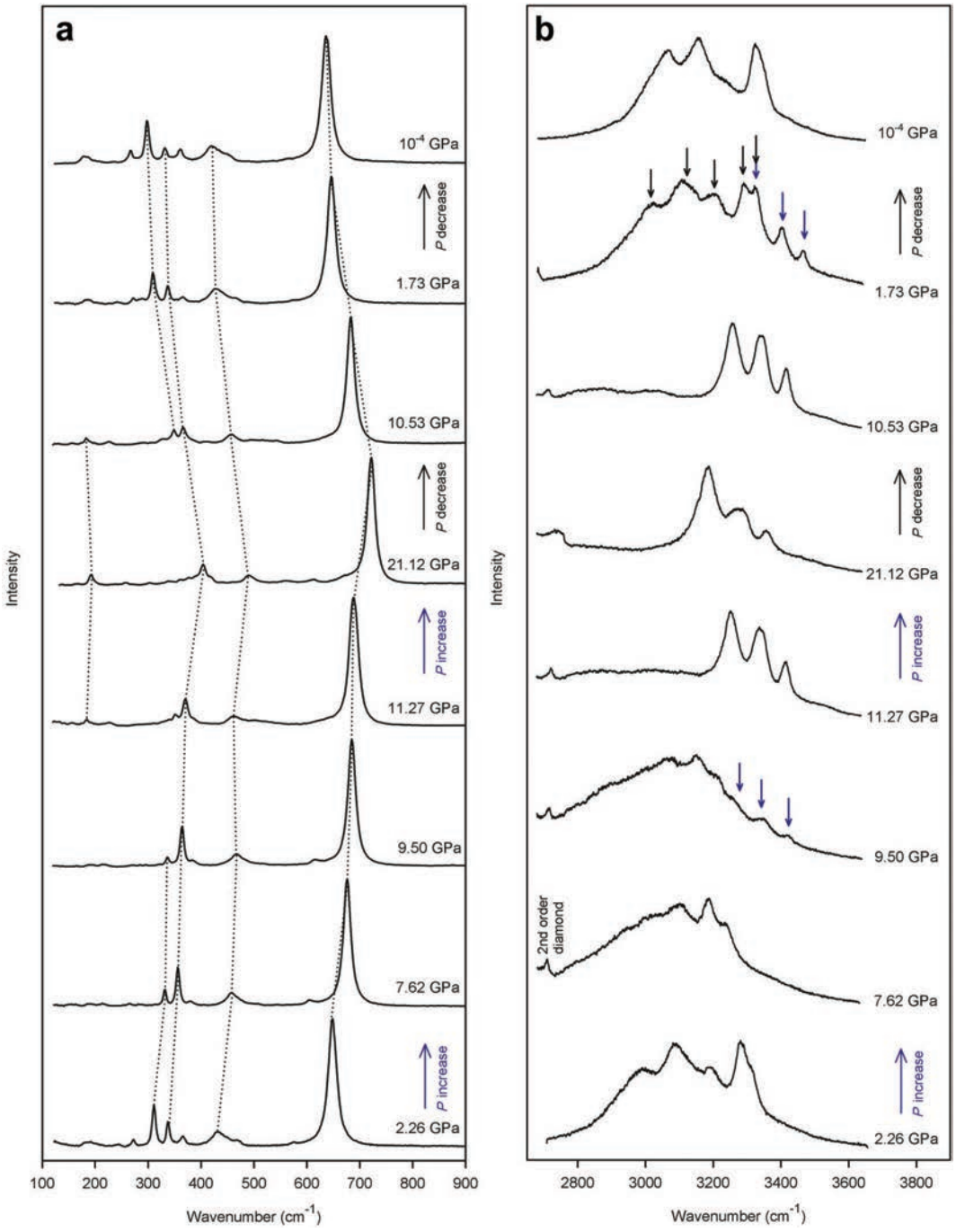

FIG. 5. Representative Raman spectra of $FeGe(OH)_6$ in the range (*a*) 100–900 cm^{-1} and (*b*) 2700–3700 cm^{-1} as function of pressure for one selected crystal-to-laser beam orientation. Spectra have been scaled for easy comparison, no background has been subtracted.

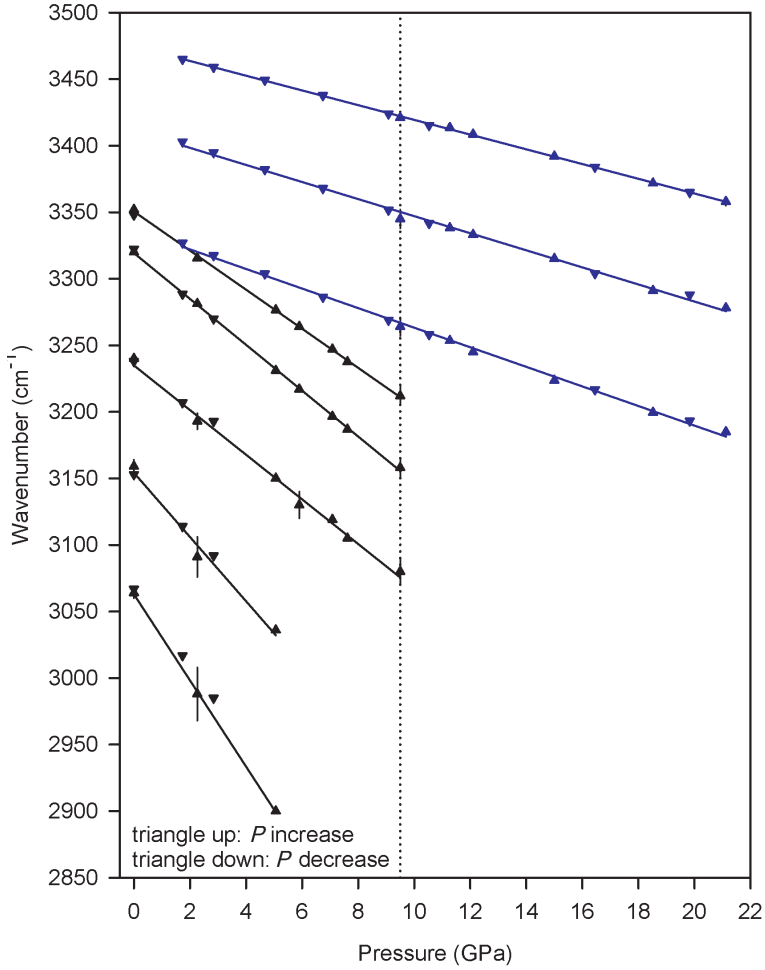

FIG. 6. The pressure dependence of the position of the OH-stretching bands in stottite. On pressure increase up to 5.1 GPa five bands are resolved (black triangles). At pressures $\geqslant$5.9 GPa the two OH bands <3200 cm^{-1} broaden and overlap significantly; at pressures $\geqslant$9.5 GPa they are no longer clearly discernable. Three pressure-induced OH-stretching bands appear at about 9.5 GPa (blue triangles). Representative error bars are given where errors are larger than the size of the symbol. Modes have been assumed to vary linearly with pressure over the investigated pressure range (solid lines). The dotted line serves as a guide for the eye.

The 11.3 GPa spectrum contains only the three new bands, with no vestiges of the original stottite spectrum. On compression to 21 GPa the three bands shift to lower wavenumber. On decompression, the three-band spectra shift to higher wavenumber. Below 10 GPa all of the spectra are mixtures of the three band and the original low pressure stottite spectra. The final ambient spectrum collected with an open DAC, is almost identical to the initial ambient spectrum. Thus, despite the hysteresis, as evidenced by mixed spectra, the spectral changes, including the FWHM line widths, are fully reversible.

Unlike the dramatic spectral changes in the OH-stretching region, the framework modes of stottite show no major changes over the full compression cycle, which shows that the main structural framework is preserved up to 21 GPa. In the range 100–900 cm^{-1} all of the observed Raman modes have a positive pressure dependence (Fig. 5*a*; Table 1) with the strongest modes being tracked reliably up to the maximum pressure.

TABLE 1. Ambient Raman frequencies and pressure derivatives of framework and OH-stretching modes of stottite. Only intense framework modes that are clearly resolved over the investigated pressures range or parts of it are listed. Modes have been assumed to vary linearly with pressure, and data points on pressure increase and decrease have been used for fitting unless otherwise indicated.

ν_i (cm^{-1})	$\partial\nu/\partial P$ (cm^{-1} GPa^{-1}) $10^{-4} \leqslant P \leqslant 9.5$ GPa	$\partial\nu/\partial P$ (cm^{-1} GPa^{-1}) $9.5 < P < 15$ GPa	$\partial\nu/\partial P$ (cm^{-1} GPa^{-1}) $15 \leqslant P \leqslant 21.12$ GPa
Framework modes			
297.2	4.17‡		
332.0	3.48		
360.5	2.82		
417.7	5.19†	−0.77†	2.95†
565.5	5.55‡		
636.2	5.20†	−0.09†	3.52†
OH-stretching bands			
3064	−32.37#		
3159	−24.13#		
3240	−16.77		
3320	−17.24		
3352	−14.68		
3336.7*	−7.35		
3414.2*	−6.87		
3473.7*	−5.53		

‡ Observed unambiguously on pressure increase up to 9.5 GPa.
† Only the frequencies on pressure increase are used for fitting the segment because the band shows a hysteresis effect on pressure release.
# Fitted at pressures $\leqslant$5.9 GPa.
* Extrapolated from high-pressure data. Modes have been observed at pressures $\geqslant$9.5 GPa on pressure increase and down to 1.73 GPa on pressure release.

Single-crystal X-ray diffraction

Crystallographic data and information about the X-ray data collection and structure determination are summarized in Table 2. Systematic absences indicate $P4_2/n$ symmetry. Reflection merging in Laue groups 1, 2/*m*, *mmm*, 4/*m* and 4/*mmm* gave R_{int} values of 0.035, 0.037, 0.093, 0.041 and 0.095, respectively. The unconstrained unit cell has a = 7.5454(5), b = 7.5553(4), c = 7.4728(6) Å, α = 89.983(5), β = 89.957(6), γ = 89.982(5)° and V = 426.00(5) Å^3. The corresponding constrained tetragonal cell has a = 7.5520(1), c = 7.4694(2) Å and V = 426.01(2) Å^3. Reconstructed pseudo-precession photos of *hk*0, *h*0*l* and 0*kl* sections of the reciprocal lattice of stottite were obtained using *Unwarp* in *CrysalisPro* (Fig. 7). The *hk*0 section has a strong $a/2$ subcell. No indications of twinning were evident in diffraction patterns.

Attempts to solve the structure by direct methods or Patterson synthesis were unsuccessful. The *E*-statistics suggested non-centrosymmetry (E = 0.741). However, attempts to determine the structure in the non-centrosymmetric space groups $P4_2$ and $P\bar{4}$, both subgroups of $P4_2/n$, were unsuccessful. Consequently, as an initial way forward we used the atom coordinates of the $P4_2/n$ structure reported by Ross *et al*. (1988) as a starting model. Full anisotropic refinement of the stottite structure in space group $P4_2/n$ proceeded smoothly to give final agreement indices of R_1 = 0.038 and wR_2 = 0.086. No H atoms were evident in difference-Fourier syntheses. Atom coordinates, and U_{ij} and U_{eq} values are listed in Table 3 and the structure is shown in Fig. 8. Bond lengths and polyhedral distortion indices (Robinson *et al*. 1971) are given in Table 4.

As indicated above, reflection merging in 4/*m* (R_{int} = 0.041) is clearly superior to merging in 4/*mmm* (R_{int} = 0.095). Consequently, merohedral twinning is unlikely to be present or significant. Although not evident from diffraction patterns, we nonetheless checked for twinning using

TABLE 2. Information relating to XRD data collections and structure refinement of stottite at 298 K in space groups $P4_2/n$ and $P2/n$.

Cell contents	$4[FeGe(OH)_6]$
Crystal system	Tetragonal
Space group	$P4_2/n$
Unit cell dimensions (Å)	a = 7.5520(1), c = 7.4694(2)
Volume (Å^3)	426.01(6)
Reflections used for cell refinement	2408
Calculated density (g cm^{-3})	3.59
Crystal size (mm)	0.086 × 0.190 × 0.202
Theta and indices range for data collection	3.81−30.16° h ±10, k ±10, l ±10
Absorption correction (μ = 10.39 mm^{-1})	Gaussian integration (face-indexing)
Transmission max/min	0.485/0.226
Completeness to θ_{max} (%)	99.6
Reflections collected	6214
Independent reflections	593
Independent reflections with $I > 2\sigma(I)$	533
R_{int} (4/m)	0.041
Completeness to θ_{max} (%)	99.6
Data/restraints/parameters	593/0/41
Goodness-of-fit on F^2	1.298
Final R indices [$I > 2\sigma(I)$]	R_1 = 0.036, wR_2 = 0.084
R indices (all data)	R_1 = 0.038, wR_2 = 0.086
Extinction coefficient	0.040(2)
Max shift/esd	0.000
Largest diff. peak and hole	0.69 and −0.51 e$^-$ Å^{-3}
Cell contents	$4[FeGe(OH)_6]$
Crystal system	Monoclinic
Space group	$P2/n$ (non-standard setting of $P2/c$)
Unit cell dimensions (Å)	a = 7.5509(2), b = 7.4695(2), c = 7.5531(2), β = 90.005(2)°
Volume (Å^3)	426.01(2)
Theta and indices range for data collection	3.81−30.16° h ±10, k ±10, l ±10
Completeness to θ_{max}	0.996
Reflections collected	6214
Independent reflections (all)	1143
Independent reflections with $I > 2\sigma(I)$	1043
R_{int} (2/m)	0.037
Data/restraints/parameters	1143/0/80
Goodness-of-fit on F^2	1.210
Final R indices [$I > 2\sigma(I)$]	R_1 = 0.040, wR_2 = 0.094
R indices (all data)	R_1 = 0.044, wR_2 = 0.096
Extinction coefficient	0.039(2)
Max shift/esd	0.000
Largest diff. peak and hole	0.90 and −0.51 e$^-$ Å^{-3}

PLATON (Spek, 2005) which indicated possible twins related by a 180° rotation about [110]. For this twin law *PLATON* calculated a batch scale factor of only 0.08 (8%) for the minor component. We attempted a twin refinement in $P4_2/n$, starting with a batch scale factor of 0.2 and using as starting atom coordinates those of the refined untwinned structure. Refinement proceeded satisfactorily and used reflection weighting and an extinction correction in the final stages. The minor twin refined to a proportion of 9% (which is close to that indicated by *PLATON*). However, slightly poorer agreement indices were obtained (R_1 = 0.040 and wR_2 = 0.134) compared with the refinement with no twinning. No clear improvement was achieved by taking into account

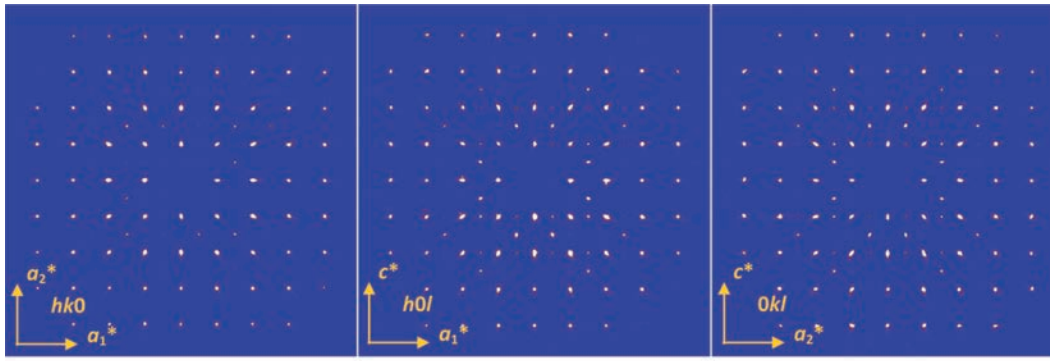

FIG. 7. Pseudo-precession *hk*0, *h*0*l* and 0*kl* images of stottite reconstructed from the intensity data collection using *Unwarp* in *CryalisPro*. A strong *a**/2 sublattice is evident in the *hk*0 section.

possible twinning. We therefore consider the case for twinning to be inconclusive, and it does not appear to affect the refined structure significantly.

As reflection merging in 2/*m* also gave a good agreement index (R_{int} = 0.037) we attempted a refinement in space group *P*2/*n* (*Z* = 4), a non-standard setting of *P*2/*c*, which is a subgroup of $P4_2/n$. We used the non-standard setting as a comparison with the $P4_2/n$ structure. Data reduction to the (pseudo-tetragonal) monoclinic unit cell gives *a* = 7.5509(1), *b* = 7.4695(2), *c* = 7.5531(2) Å, β = 90.005(2)° and *V* = 426.01(2) Å^3. As structure solution was unsuccessful, we used the *Powdercell* program to derive an initial unique model *P*2/*n* structure (*Z* = 4) for refinement, that is derived from a stottite-like pseudo-tetragonal structure. The refinement proceeded smoothly to give final values R_1 = 0.044 and wR_2 = 0.096 and a reasonable structure. No H atoms were found in the difference-Fourier maps. Experimental details of the refinement in *P*2/*n* are given in Table 2 and atom coordinates and displacement parameters in Table 3. The refined *P*2/*n* structure is shown in Fig. 8. It has a +–+ tilt system which is analogous to ++– of stottite. Compared with $P4_2/n$, the *P*2/*n* structure has all its atom sites doubled, with six non-equivalent oxygen atoms: Ge(1,2), Fe(1,2) and O(1−6). Thus, it is consistent with the six OH bands of the 150 and 300 K Raman spectra. Finally, it should be noted that refinement in the monoclinic space group $P2_1/n$ failed. Thus, *P*2/*n* is the only plausible alternative to $P4_2/n$ as the ambient structure of stottite; *P*2/*n* is preferred over $P4_2/n$ on the grounds that it allows for six OH bands in the Raman spectrum.

Discussion

The ambient and 150 K Raman spectra of stottite in the OH-stretching region are inconsistent with the $P4_2/n$ structure determined by Strunz and Giglio (1961), Ross *et al*. (1988) and ourselves. In this respect the reservations expressed by Ross *et al*. (1988) are relevant: "... the unit-cell symmetry appeared lower than tetragonal – either orthorhombic or, more likely, monoclinic (based on subgroup relations) with β ~90°. For neither crystal was the evidence so convincing as to force refinement in a lower symmetry than $P4_2/n$, but the discrepancies were a trifle disturbing, particularly considering the anomalous optical properties previously mentioned." Thus, there are grounds for uncertainty concerning the space group of stottite as determined by XRD.

Our refinement in *P*2/*n* converged to give a reasonable result, and the structure is topologically similar to that of $P4_2/n$ stottite. The non-H *P*2/*n* structure has a clear tetragonal pseudosymmetry that may not be possible to resolve conclusively using X-ray diffraction. However, the *P*2/*n* result indicates that such a structure, which has six non-equivalent oxygen atoms, is consistent with the diffraction data. Thus, a critical link with the Raman spectra has been identified and this allows us to propose a phase transition from $P2/n \rightarrow P4_2/n$ on compression. Taking the XRD and Raman results together, we propose that stottite has the *P*2/*n* structure at ambient conditions.

Some insight into the structural subtleties of stottite and the potential difficulties associated with strong pseudosymmetries in hydroxide-perovskites, can be gained from a recent study

TABLE 3*a*. Atom coordinates, anisotropic and equivalent-isotropic displacement parameters of $P4_2/n$ stottite at 293 K.

Site	*x/a*	*y/a*	*z/c*	U_{11}	U_{22}	U_{33}	U_{23}	U_{13}	U_{12}	U_{eq}
Ge	½	0	½	0.0065(4)	0.0069(4)	0.0068(4)	−0.0001(2)	−0.0001(2)	0.0000(2)	0.0067(3)
Fe	½	0	0	0.0078(4)	0.0074(4)	0.0081(5)	0.0002(3)	−0.0001(3)	0.0001(3)	0.0078(3)
O(1)	0.2670(4)	0.0552(4)	0.5825(4)	0.008(1)	0.013(1)	0.015(2)	−0.001(1)	−0.001(1)	0.001(1)	0.0121(7)
O(2)	0.5708(4)	0.2317(4)	0.5638(4)	0.012(1)	0.008(1)	0.015(2)	−0.002(1)	−0.002(1)	0.000(1)	0.0119(7)
O(3)	0.5637(4)	−0.0763(4)	0.7329(4)	0.012(1)	0.011(1)	0.008(1)	0.001(1)	−0.000(1)	0.001(1)	0.0102(6)

Table 3*b*. Atom coordinates, anisotropic and equivalent-isotropic displacement parameters of $P2/n$ stottite at 293 K.

Site	*x/a*	*y/b*	*z/c*	U_{11}	U_{22}	U_{33}	U_{23}	U_{13}	U_{12}	U_{eq}
Ge(1)	0	½	0	0.0064(3)	0.0070(3)	0.0069(3)	0.0002(2)	0.0002(2)	0.0002(2)	0.0068(2)
Ge(2)	½	0	0	0.0065(3)	0.0068(3)	0.0064(3)	0.0002(2)	0.0004(2)	−0.0001(2)	0.0066(2)
Fe(1)	0	0	0	0.0076(4)	0.0079(4)	0.0080(4)	−0.0003(3)	0.0001(3)	0.0000(3)	0.0078(2)
Fe(2)	½	½	0	0.0075(4)	0.0077(4)	0.0081(4)	0.0003(3)	0.0000(3)	0.0002(3)	0.0078(2)
O(1)	0.2675(4)	0.5826(4)	0.5548(4)	0.009(1)	0.014(2)	0.014(1)	0.001(1)	0.001(1)	−0.001(1)	0.0122(6)
O(2)	0.5553(4)	0.0826(4)	0.2330(4)	0.014(2)	0.014(2)	0.009(1)	0.001(1)	−0.001(1)	−0.002(1)	0.0126(6)
O(3)	−0.4290(4)	0.5639(4)	0.7316(4)	0.012(1)	0.015(2)	0.009(1)	−0.002(1)	0.000(1)	−0.002(1)	0.0120(6)
O(4)	−0.2689(4)	0.0640(4)	0.9290(4)	0.009(1)	0.014(2)	0.013(2)	0.002(1)	0.000(1)	−0.003(1)	0.0120(6)
O(5)	−0.5639(4)	0.2672(4)	0.5762(4)	0.0121(1)	0.007(1)	0.011(1)	0.001(1)	0.000(1)	0.000(1)	0.0100(6)
O(6)	0.5765(4)	0.7672(4)	0.0634(4)	0.008(1)	0.012(1)	0.008(1)	0.011(1)	0.001(1)	0.001(1)	0.0100(6)

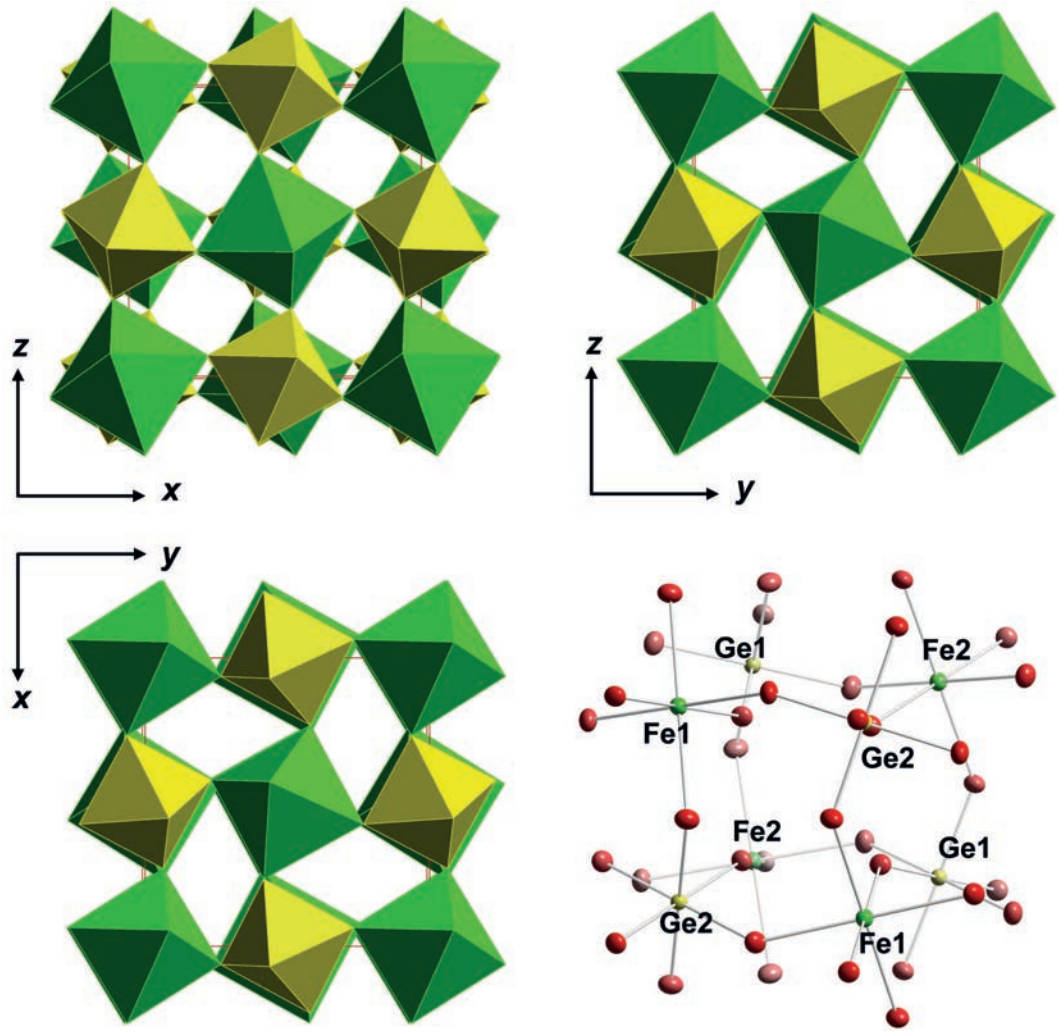

FIG. 8. The non-H structure of *P*2/*n* stottite determined in this study. The atomic configuration around a single empty A-site cavity is shown (one-eighth of the unit cell). Atom displacement ellipsoids are shown at the 68% level.

of the synthetic hydroxide-perovskite $MgSi(OH)_6$, also known as the "3.65 Å-phase", by Wunder *et al*. (2011). Its structure was inferred by comparison with the X-ray powder diffraction pattern of δ-$Al(OH)_3$ (Matsui *et al*. 2011), and using Rietveld refinement to obtain structural data in orthorhombic space group *Pnam* (Z = 2) as follows: a = 5.1900(3), b = 5.1132(3), c = 7.3304(4) Å and V = 194.53(2) Å^3. However, two low-angle diffraction peaks of significant intensity were not fitted by the *Pnam* model. Furthermore, the infrared spectrum in the OH-stretching region of $MgSi(OH)_6$ contains six absorption bands, and is inconsistent with *Pnam* symmetry (three non-equivalent OH groups).

Wunder *et al*. (2012) reported the results of a computational study of $MgSi(OH)_6$ using density-functional theory (DFT) in which they proposed that the most likely space group was $P2_1$ (monoclinic), with six non-equivalent OH groups, this being consistent with the infrared OH-stretching spectra. This structure is metrically pseudo-orthorhombic with β = 90.03(1)º. Crucially, the $P2_1$ structure has an ordered

TABLE 4. A comparison of parameters of the different stottite structural models.

$P4_2/n$ structure		$P2/n$ structure			
Ge		Ge(1)		Ge(2)	
O1	1.910(3)	O1	1.907(3)	O2	1.911(3)
O2	1.891(3)	O3	1.890(3)	O4	1.888(3)
O3	1.895(3)	O5	1.894(3)	O6	1.894(3)
<Ge−O>	1.899	<Ge(1)−O>	1.897	<Ge(2)−O>	1.898
V	9.213	V	9.098	V	9.102
σ^2	1.026	σ^2	1.18	σ^2	1.177
<λ>	1	<λ>	1	<λ>	1
Fe		Fe(1)		Fe(2)	
O1	2.150(3)	O2	2.150(3)	O1	2.152(3)
O2	2.150(3)	O4	2.154(3)	O3	2.151(3)
O3	2.132(3)	O5	2.132(3)	O6	2.132(3)
<Fe−O>	2.147	<Fe(1)−O>	2.145	<Fe(2)−O>	2.145
V	13.153	V	13.134	V	13.123
σ^2	8.184	σ^2	5.716	σ^2	6.018
<λ>	1.002	<λ>	1.002	<λ>	1.002

alternation of $Mg(OH)_6$ and $Si(OH)_6$ octahedra, whereas the *Pnam* structure has a single mixed cation site, implying Mg−Si disorder.

A structure determination of $MgSi(OH)_6$ using single-crystal XRD on coarse, well crystallized material synthesized at 10 GPa and 450ºC for 205 h has been reported by Welch and Wunder (in press). The structure is monoclinic $P2_1/n$ (Z = 2), but metrically pseudo-orthorhombic, with a = 5.11606(9), b = 5.19282(9), c = 7.33434(14) Å, β = 90.021(2)º and V = 194.850(6) Å^3. However, a few weak violators of the *n*-glide were observed, consistent with a $P2_1$ component. Refinements of the structure in $P2_1$ were problematic and unstable (non-convergence; non-positive-definite values for several oxygen U_{ij}s; and very large standard errors on the Flack parameter). Consequently, the X-ray-based structure has space group $P2_1/n$, which has three non-equivalent H atoms. The very weak X-ray signature of the $P2_1$ structure may reflect very similar non-H structures for the two phases, and also the fact that the primary distinction is due to H location, which is registered by Raman and infrared spectroscopy, but not by XRD.

A comparison of the Raman spectra of stottite and the infrared spectrum of $MgSi(OH)_6$ (Wunder *et al*., 2011, fig. 2*a*) is instructive. The 150 K and ambient spectra of stottite have six OH-absorption bands and are qualitatively very similar to the ambient infrared spectrum of $MgSi(OH)_6$. The wavenumber shifts between the two studies reflect the different nearest-neighbour cations bonded to OH groups: Fe−O(H)−Ge *vs*. Mg−O(H)−Si. The close correspondence of the stottite and $MgSi(OH)_6$ spectra suggests that the OH groups of $P2_1$ (Z = 2) $MgSi(OH)_6$ and $P2/n$ (Z = 4) stottite occupy analogous local environments. Hence, by analogy with the high-pressure behaviour of stottite, a transition $P2_1 \rightarrow P2_1/n$ in $MgSi(OH)_6$ on compression seems likely. Such a transition could be identified as a change from six to three OH bands in Raman or infrared spectra.

A further interesting subtlety concerning the transitional behaviour of stottite is the apparent hysteresis, particularly on decompression. We have no evidence for significant pressure variation within the DAC and the irradiated sample area was 0.01 mm in diameter, and so we infer that the observed mixed spectra, implying two coexisting phases, reflect the nature of the phase transition. Thermal hysteresis has been observed in first-order phase transitions in numerous materials, including perovskites. In the present case, the hysteresis involves pressure rather than temperature. The origin of hysteresis in stottite, and its possible existence in related hydroxide-perovskites, merits further study.

Conclusive structural data for stottite, at ambient conditions and at high pressure, are highly desirable, but obtaining these data from

X-ray diffraction is not a trivial task. It appears that pseudosymmetry in some hydroxide-perovskites presents problems for definitive structure determination, even though high-quality structure refinements from XRD can be obtained. In H-rich structures, such as hydroxide-perovskites, with their extensive H-bonded connectivity throughout the octahedral framework, H behaviour may have a significant role in phase transitions. In this regard, spectroscopic studies are likely to provide key information on symmetry breaking in hydroxide-perovskites, as registered by the OH-stretching region.

Acknowledgements

This work was supported by Natural Environment Research Council fellowship NER/I/S/2001/00723 and Natural Environment Research Council grant NER/B/S/2003/00258 to AKK, and Natural Environment Research Council grants GT59801ES and GR3/10912 to APJ; MDW and WAC thank the ESRF for beam time.

References

Basciano, L.C., Peterson, R.C. and Roeder, P.L. (1998) Description of schoenfliesite, $MgSn(OH)_6$, and roxbyite, $Cu_{1.72}S$, from a 1375 BC shipwreck, and Rietveld neutron-diffraction refinement of synthetic schoenfliesite, wickmanite, $MnSn(OH)_6$, and burtite, $CaSn(OH)_6$. *The Canadian Mineralogist*, **36**, 1203–1210.

Birch, W.D., Pring, A., Reller, A. and Schmalle, H.W. (1993) Bernalite, $Fe(OH)_3$, a new mineral from Broken Hill, New South Wales: description and structure. *American Mineralogist*, **78**, 827–834.

Jephcoat, A.P., Mao, H.K. and Bell, P.M. (1987) Operation of the Megabar Diamond-Anvil Cell. *Hydrothermal Experimental Techniques*, **19**, 469–506.

Matsui, M., Komatsu, K., Ikeda, E., Sano-Furukawa, A., Gotou, H. and Yagi, T. (2011) The crystal structure of δ-$Al(OH)_3$: neutron diffraction measurements and *ab initio* calculations. *American Mineralogist*, **96**, 854–859.

Robinson, K., Gibbs, G.V. and Ribbe, P.H. (1971) Quadratic elongation: a quantitative measure of distortion in coordination polyhedra. *Science*, **172**, 567–570.

Ross C.R. II, Bernstein, L.R. and Waychunas, G.A. (1988) Crystal-structure refinement of stottite, $FeGe(OH)_6$. *American Mineralogist*, **73**, 657–661.

Ross, N.L., Chaplin, T.D. and Welch, M.D. (2002) Compressibility of stottite, $FeGe(OH)_6$: an octahedral framework with protonated O atoms. *American Mineralogist*, **87**, 1410–1414.

Ross, N.L., Zhao, J., Burt, J.D. and Chaplin, T.D. (2004) Equations of state of $GdFeO_3$ and $GdAlO_3$ perovskites. *Journal of Physics, Condensed Matter*, **16**, 5721–5730.

Sheldrick, G.M. (2008) A short history of *SHELX*. *Acta Crystallographica*, **A64**, 112–122.

Spek, A.L. (2005) *PLATON, A multipurpose crystallographic tool*. Utrecht University, Utrecht, The Netherlands.

Strunz, H. and Giglio M. (1961) Die Kristallstruktur von Stottite, $Fe[Ge(OH)_6]$. *Acta Crystallographica*, **14**, 205–208.

Strunz, H., Söhnge, G. and Geier, B. H. (1958) Stottite, ein neues Germanium-Mineral und seine Paragenese in Tsumeb. *Neues Jahrbuch für Mineralogie Monatshefte*, **1958**, 85–96.

Welch, M.D. and Wunder, B. (in press) A single-crystal X-ray diffraction study of the 3.65 Å-phase $MgSi(OH)_6$, a high-pressure hydroxide perovskite. *Physics and Chemistry of Minerals*, http://dx.doi.org/10.1007/s00269-012-0523-y.

Welch, M.D., Crichton, W.A. and Ross, N.L. (2005) Compression of the perovskite-related mineral bernalite $Fe(OH)_3$ to 9 GPa and a reappraisal of its structure. *Mineralogical Magazine*, **69**, 309–315.

Williams, S.A. (1985) Mopungite, a new mineral from Nevada. *Mineralogical Record*, **16**, 73–74.

Wunder, B., Wirth, R. and Koch-Müller, M. (2011) The 3.65 Å phase in the system $MgO–SiO_2–H_2O$: synthesis, composition, and structure. *American Mineralogist*, **96**, 1207–1214.

Wunder, B., Jahn, S., Koch-Müller, M. and Speziale, S. (2012) The 3.65 Å phase, $MgSi(OH)_6$: structural insights from DFT calculations and *T*-dependent IR spectroscopy. *American Mineralogist*, **97**, 1043–1048.

Zhao, J., Ross, N.L. and Angel, R.J. (2004) A new view of the high-pressure behaviour of $GdFeO_3$-type perovskites. *Acta Crystallographica*, **B60**, 263–271.